Eur. Phys. J. B **36**, 431–443 (2003)
DOI: 10.1140/epjb/e2004-00001-9

THE EUROPEAN PHYSICAL JOURNAL B

Interferential polychromatic filters

M. Kanzari[a], A. Bouzidi, and B. Rezig

Laboratoire de Photovoltaïque et Matériaux Semiconducteurs (LPMS), École Nationale d'ingénieurs de Tunis-BP 37 le Belvédère 1002 Tunis, Tunisia

Received 10 July 2003
Published online 30 January 2004 –

Abstract. The reflection properties of one-dimensional generalized Cantor-like multilayer (GCLM) are investigated numerically in the visible range. Strong correlation between the stack geometry and the properties of the optical reflection spectra is found, namely spectral scalability and sequential splitting. The construction of multilayer systems according to the definite Cantor distribution brings improvements to the reflection properties. In particular, the widening of the band gap and the thin peak appearance in the reflection spectra whose number increases with the division number in the (GCLM). Optical properties of (GCLM) inserted between two periodic stacks are numerically investigated. We chose SiO_2(L) and TiO_2 (H) as two elementary layers. The study configuration is $H(LH)^5[GCLM]^P H(LH)^5$ which forms an effective interferential filter in the visible spectral range. We show that the number of resonator peaks is dependent on the repetition of the number P of the (GCLM). The best performances are obtained in particular for the symmetrical configurations of the (GCLM) and especially for P an odd number.

PACS. 61.44.Br Quasicrystals – 42.70.Qs Photonic bandgap materials – 42.79.Ci Filters, zone plates, and polarizers

1 Introduction

During the last decade, one dimensional dielectric structures, referred to as photonic crystals, have been extensively studied both theoretically and experimentally [1–7]. Photonic band gap (PBG) crystals are usually composed of altering layers having a high refractive index say n_H, and a low refractive index say n_L, in an arrangement that gives rise to a series of forbidden wavelength gaps. That is, light is almost completely reflected by the crystal, while a series of wavelength pass bands form [8].

It has been shown that for a suitable choice of high and low refractive indices n_H, and n_L, periodic structures strongly reflect at frequencies and angles of incidence corresponding to photonic band gap [9]. On the other hand, PBGs have been extended to photonic quasiperiodic structures [10–12] such as Cantor and Fibonacci multilayer.

This work deals with the use of quasiperiodic structures for novel optical components. We first report a numerical simulation of the reflection properties of multilayer films, built according to the asymmetrical Cantor mode proposed here. The construction of multilayer systems according to the Cantor distribution brings improvements in the reflection properties. Indeed, this model will allow the construction of fractal multilayer structures with the aim of getting more interesting optical properties by comparison with the results obtained with classic periodic PBG structures. Secondly, we intend to study an interferential filter based on the generalized Cantor-like multilayer. The generalized Cantor-like multilayer represents an interest polychromatic filter when is sandwiched between two periodic stacks [13].

2 Generalized Cantor-like multilayer

To built multilayer structures according to this model, we start from an initiator of length l and of high refractive index n_H, we subdivide it into m unities of equal length (l/m), the first layer of length $a(l/m)$ is a layer of high refractive index n_H, the second layer of length $b(l/m)$ is a layer of low refractive index n_L and the last layer of length $[l-(a+b)l/m]$ is of high refractive index n_H. Where a and b are integer, m the homothetic ratio. If $m=2$ the interferential mirror is a periodic multilayer. When $m>2$, we have to consider different cases according to the algebraic properties of the homothetic ratio. This is the first step ($N=1$) of the model. In the second iteration ($N=2$), we subdivide into m units of equal length $a(l/m^2)$, the first layer and take a segment of length $a^2(l/m^2)$ as a layer of high refractive index n_H, the second layer of length $ba(l/m^2)$ is a layer of low refractive index n_L and the last layer of

[a] e-mail: mounir.kanzari@ipeit.rnu.tn

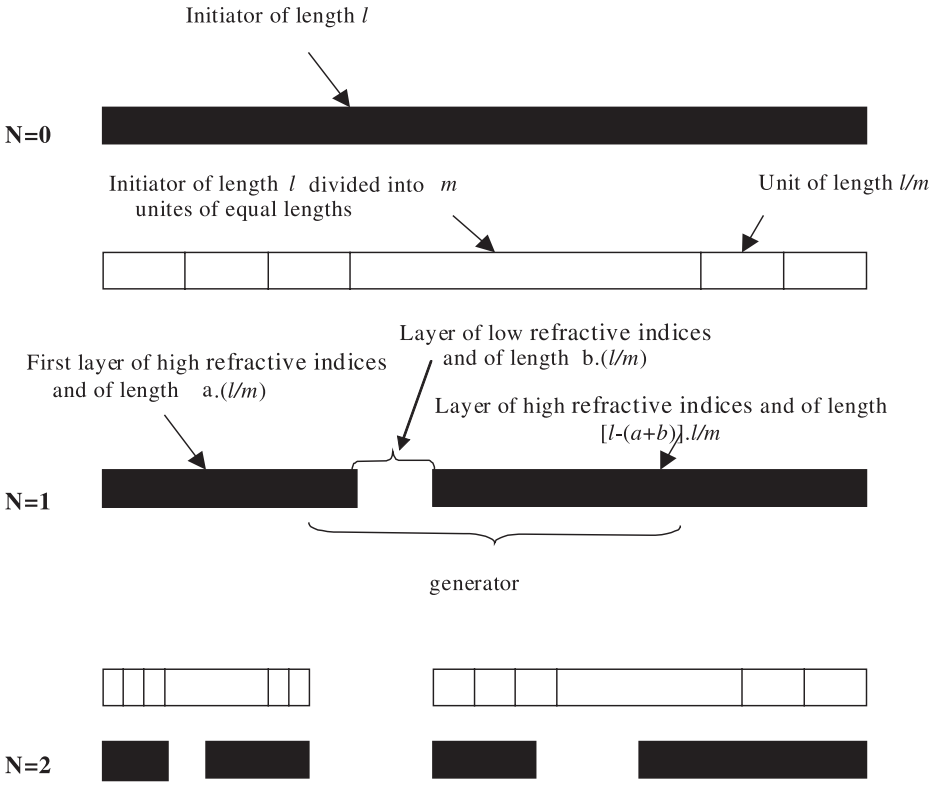

Fig. 1. The model of the generalized Cantor set construction.

length $[al/m - (a+b)(a^2l/m^2)]$ is of high refractive index n_H. We repeat this procedure for the $[l-(a+b)(l/m)]$ high refractive index layer. We subdivide it into m unities of equal length $([l-(a+b)l/m])/m$, the first layer of length $a([l-(a+b)(l/m)])/m)$ is a layer of high refractive index n_H, the second layer of length $b([l-(a+b)l/m])/m)$ is a layer of low refractive index n_L and the last layer of length: $\{l-(a+b)(l/m)-(a+b)([l-(a+b)(l/m)])/m\}$ is of high refractive index n_H as shown in Figure 1, and continuing this procedure ad infinitum. We note that a, b and m obey to: $a+b<m$.

Also notice that, within fixing $m=3$ and $(a,b)=(1,1)$, we find the classical Cantor set [7,14], and we obtain the symmetrical structures HLH for the first level $N=1$, and HLH3LHLH for the second level $N=2$ etc. Our choice for the number in the Cantor prefractal level $N=3$, is restricted because the total optical path increases for the Cantor-like multilayer of level N.

3 Interferential polychromatic filters

We now study the transmission properties of one dimensional photonic band gap structures which are built according to the pattern of generalized Cantor-like multilayer (GCLM). This structure inserted between two periodic stacks shows interesting transmission properties leading to novel optical applications such as polychromatic

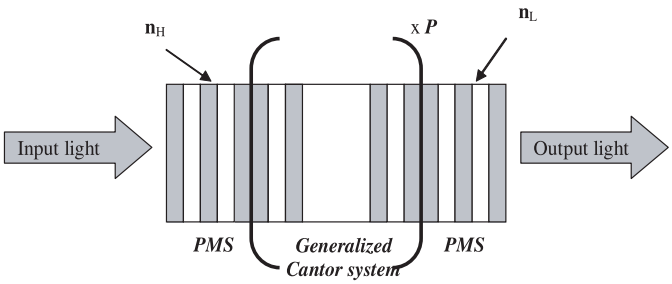

Fig. 2. The model of the study configuration $H(LH)^5[GCLM]^P H(LH)^5$.

filters. The main idea [13] consists in the insertions of the (GCLM) between two identical periodic multilayer structures (PMS) as shown in Figure 2.

The configuration is the following: $(PMS)^J[GCLM)]^P \times(PMS^J)$ where P and J are respectively, the repetition numbers of the (GCLM). and the (PMS).

The interferential filters are composed of multiple thin layers and function on the same principle that an interferometer of Fabry-Pérot. The incident light undergoes multiple reflections between the different surfaces defining resonant cavities. Interferences that occur between the different emerging bundles create a maximum in transmission when the optic path difference is an integer number of

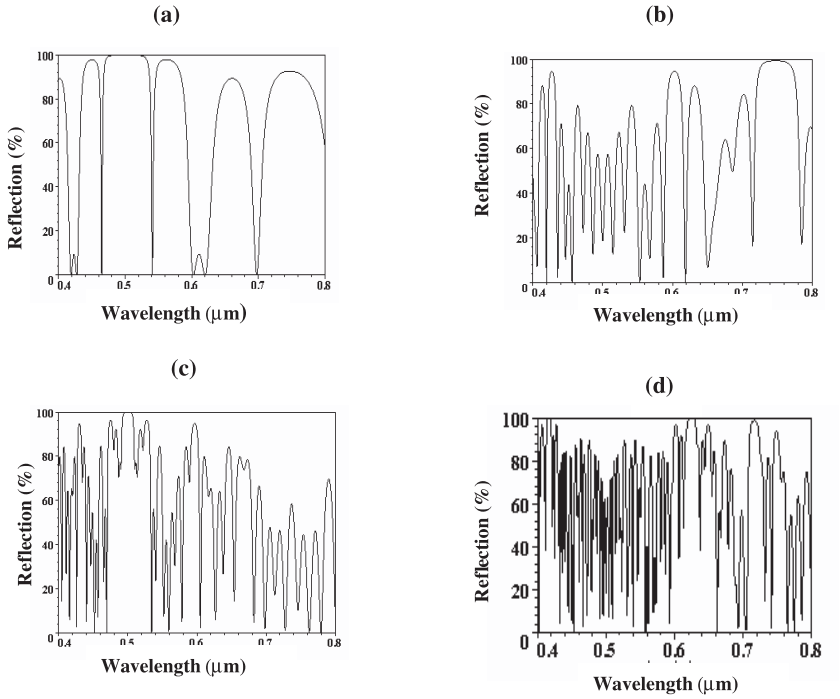

Fig. 3. The reflection properties for $(a, b) = (1, 1)$ and m an integer equal to (a): 3, (b): 4, (c): 5 and (d): 6.

the wavelength. For the other wavelengths, interferences are destructive and the transmission is very weak.

A classical Fabry-Pérot uses a space of air between reflective surfaces. An interferential filter uses a thin dielectric material layer. Reflective layers are composed of a blade stacking quarter of wave constituted of alternated materials with high and low refractive indices, permitting to reach reflectivity rates of 99.99%. Generally, filters, which are considered as interferential photonic filters, are composed of several cavities in order to get some transmission strips with the stepper sides.

4 Results and discussion

Notice that, in the following numerical simulation, we chose SiO_2 (L) and TiO_2 (H) as two elementary layers, with refractive index $n_L = 1.45$ and $n_H = 2.3$ at 700 nm, respectively. We assume that the optical indices of the dielectric layers are constant versus the wavelength for the visible domain (0.4–0.8) μm. The optical thicknesses of the two components (L) and (H) are written in the form $n_H d_H = n_B d_B = \frac{\lambda_0}{4}$, d_H and d_L are the physical thicknesses for the high index material (TiO_2) and for the low index material (SiO_2) respectively. The central wavelength λ_0 was chosen as 0.5 μm. These conditions imply the phase $\varphi = \frac{\pi}{2}\frac{\lambda_0}{\lambda}$.

4.1 Reflection properties of the (GCLM)

To evaluate the reflection spectra at a normal incidence, we use the matrix method introduced by Abeles [14] in application to the stratified multilayer structures to calculate the different photometric properties.

Figure 3 shows the reflection properties for $(a, b) = (1, 1)$ and m an integer equal to 3, 4, 5 and 6. We note the increase of the Bragg peak numbers with the increase of the homothetic ratio m. The same result for $(a,b)=(1,1)$ is also observed for m a rational and irrational number as shown in Figures 4 and 5. Figure 6 illustrates this behaviour and shows a linear variation of the Bragg peak numbers with m particularly from $m \geq 3$. The most important features of the represented spectra of the Figures 3, 4 and 5 are the following. First of all, the values of the reflection in the whole visible region are the highest for m an integer and rational. The second feature consists in the presence of many weaker band gaps in the studied spectral domain. One of the most interesting phenomena appearing in fractal materials is wave localization, so that the field becomes spatially confined in some suitable regions [15]. This property makes fractal materials very attractive from an optical point of view. The third feature, the photonic band gap at 100% reflection exists only for the integer values of m as shown in Figure 7. Consequently, we restricted our study only for the integer values of m. We fixed firstly $a = 1$ and made b vary from 1 to 4, secondly we fixed $b = 1$ and made a vary from 1 to 4. We chose $m = 6$ so as to appreciate the effect of parameters a and b. In Figures 8 and 9 we present the results of the numerical analysis of the reflection. As a general trend it can be seen that by increasing the low refractive index layers L of the sequences, more and more photonic band gaps at 100% reflection develop as shown in Figure 10

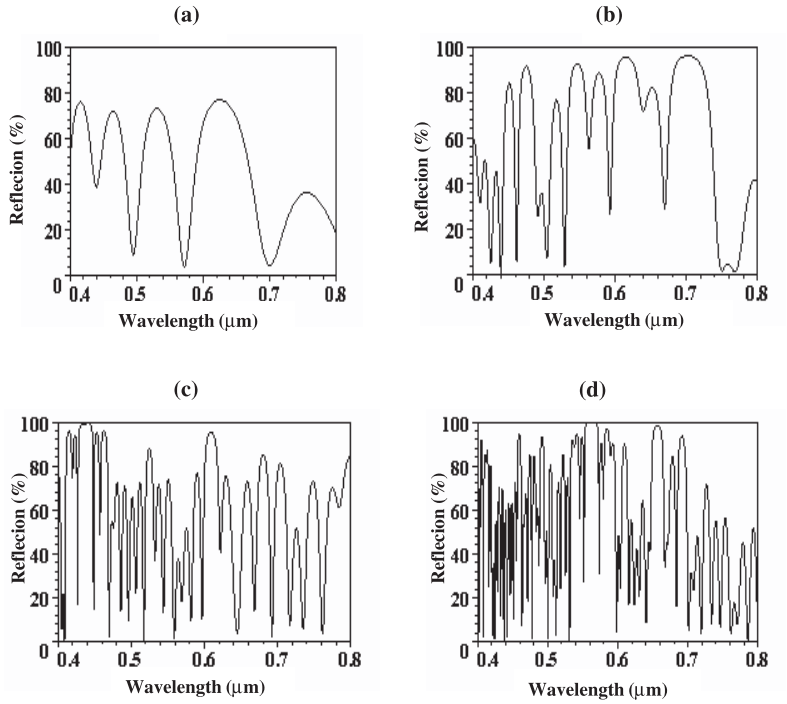

Fig. 4. The reflection properties for $(a, b) = (1, 1)$ and m a rational equal to (a):2.5, (b): 3.5, (c): 4.5 and (d): 5.5.

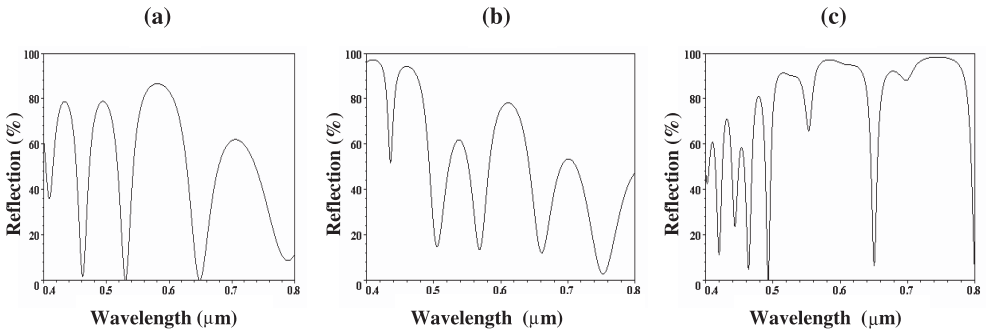

Fig. 5. The reflection properties for $(a, b) = (1, 1)$ and m an irrational equal to (a): $\sqrt{2}+1$, (b): $\sqrt{3}+1$ and (c): $\sqrt{5}+1$.

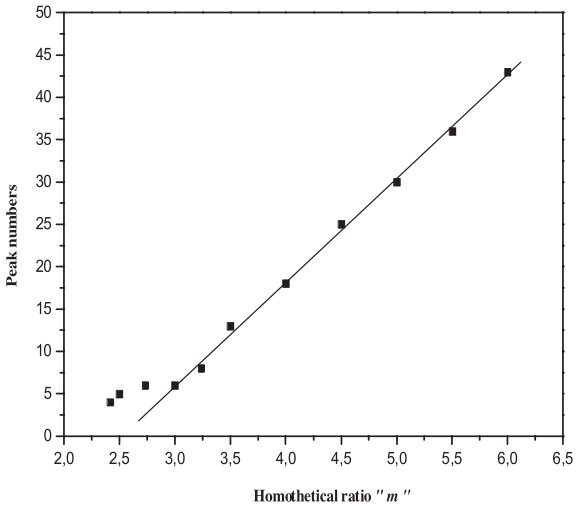

Fig. 6. Plots of the Bragg peak numbers versus the homothetic ratio m.

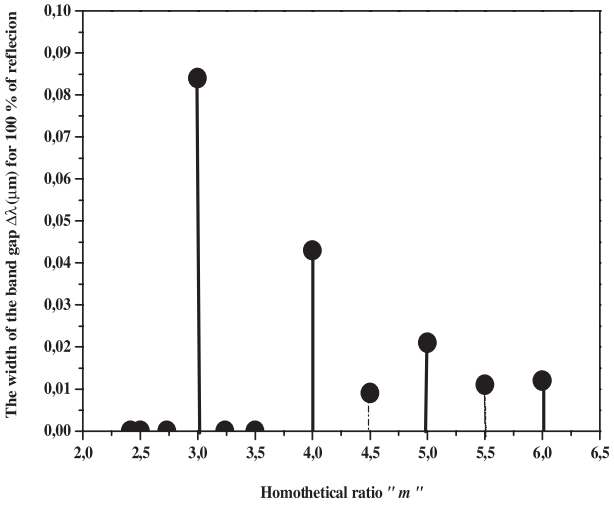

Fig. 7. Plots of the width photonic band gap at 100% reflection versus the homothetic ratio m.

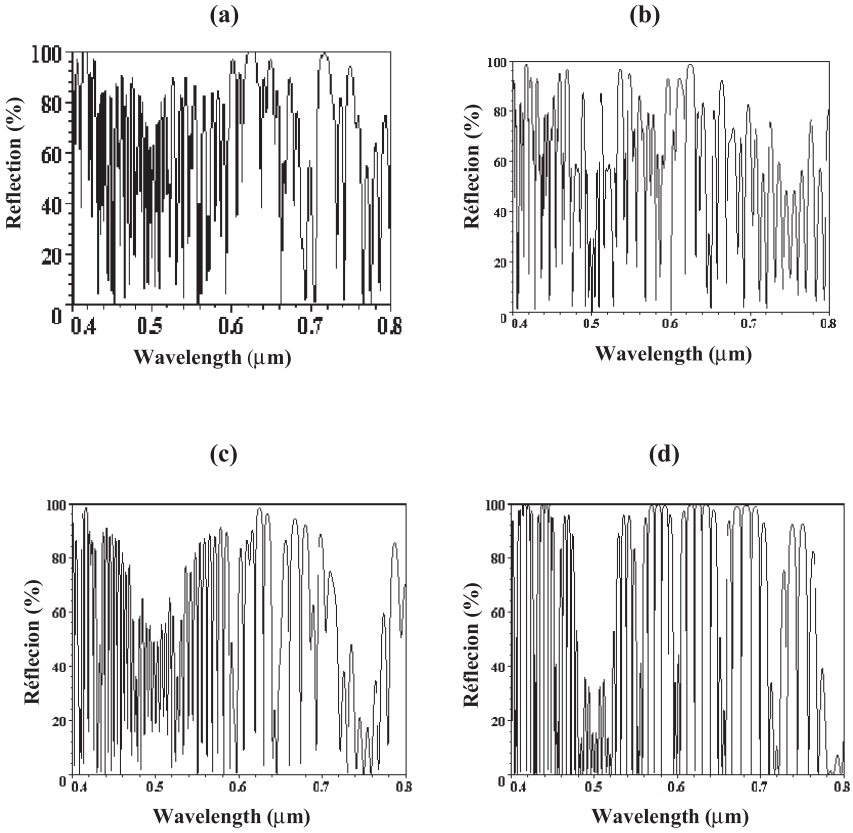

Fig. 8. The reflection properties for $m = 6$ and $(a, b) = (1, b)$ with b equal to (a): 1, (b): 2, (c): 3 and (d): 4.

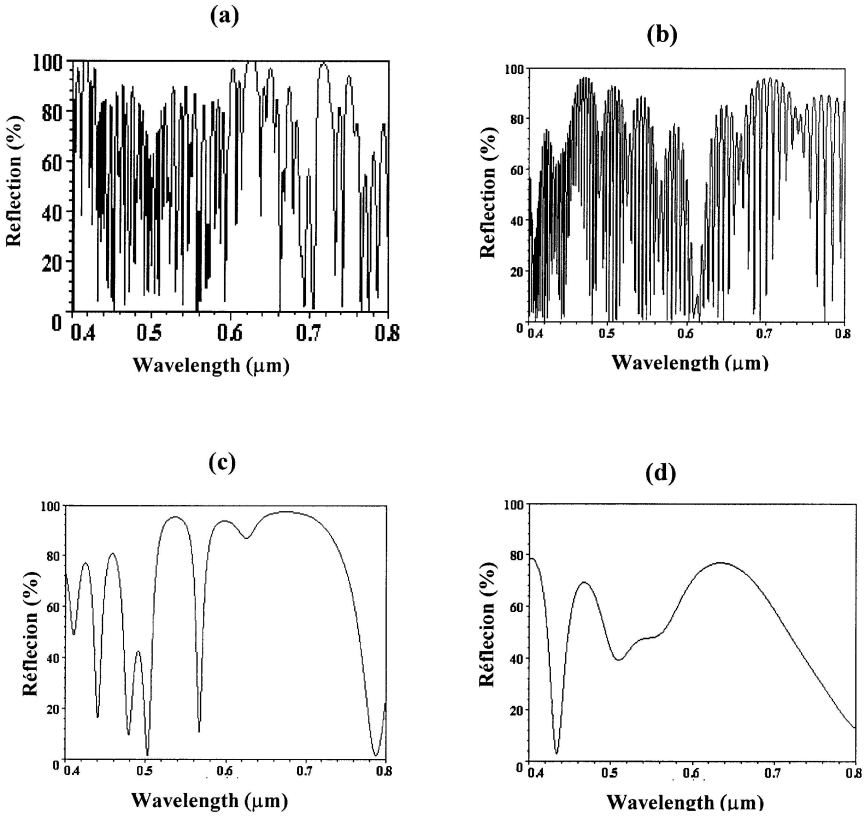

Fig. 9. The reflection properties for $m = 6$ and $(a, b) = (a, 1)$ with a equal to (a): 1, (b): 2, (c): 3 and (d): 4.

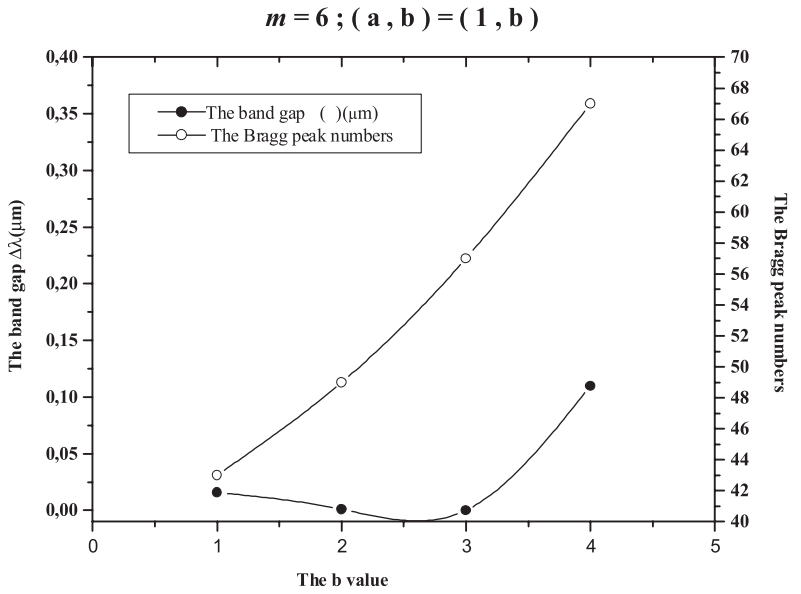

Fig. 10. Plots of the width photonic band gap at 100% reflection and the Bragg peak numbers versus the integer b for $m = 6$ and the third iteration.

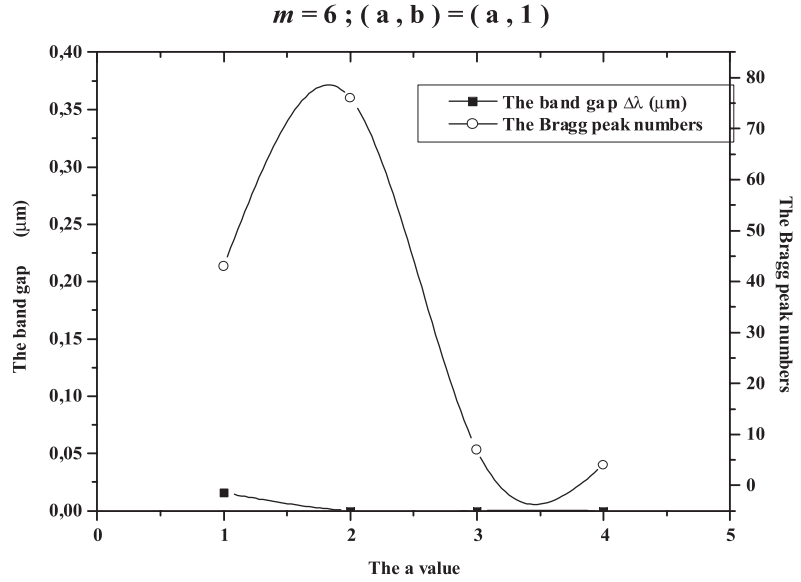

Fig. 11. Plots of the width photonic band gap at 100% reflection and the Bragg peak numbers versus the integer a for $m = 6$ and the third iteration.

which summarizes the results of the Figure 8. This result is encouraging as regards the possible use of these effects in optical devices since the Bragg peaks are accompanied by the transmission dips. Therefore, these configurations can be used as a perfect polychromatic filter when they are sandwiched between the periodic stacks [13]. On the contrary when the high refractive index layers H increase, the number of Bragg peaks and the width of the photonic band gap at 100% reflection decrease as shown in Figure 11, which summarizes the results of the Figure 9. Finally, it is crucial to note, that the interesting results are obtained particularly for m an integer and b higher than a.

4.2 Transmissions properties of the $(PMS)^J[GCLM)]^P(PMS)^J$ structures

4.2.1 The optimisation of the repetition number J of the (PMS)

In order to optimize the value of the repetition number J of the periodic multilayer structures (PMS),

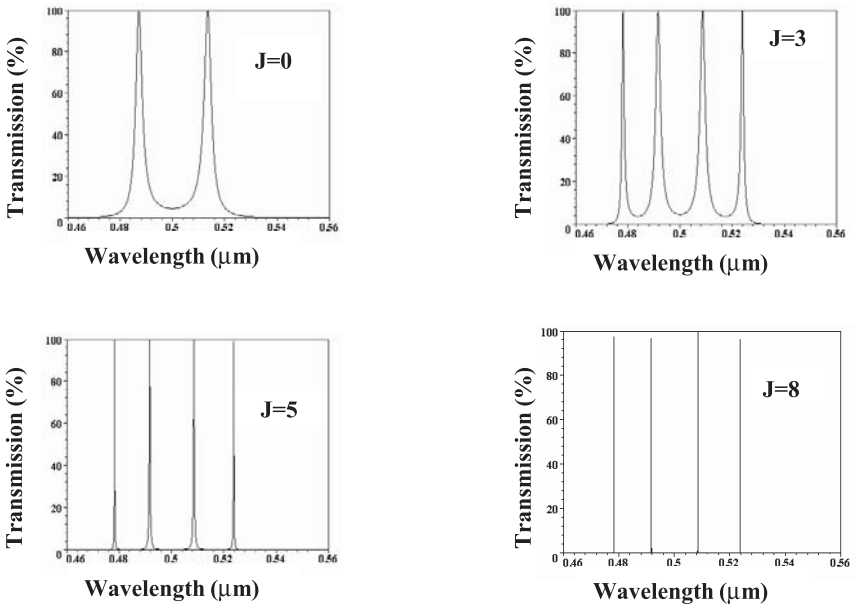

Fig. 12. Transmission spectrum versus wavelength for the $H(LH)^J(HLH3LHLH)^3H(LH)^J$ structure for different J values.

we studied in the range 0.46–0.52 μm and at normal incidence the optical transmission of the system $H(LH)^J(HLH3LHLH)^PH(LH)^J$ where H and L are the elementary layers SiO_2 (L) and TiO_2 (H) with refractive index $n_L = 1.45$ and $n_H = 2.3$ at 700 nm, respectively. Then, we fixed P to 3 and let J vary from 0 to 8. Figure 12 presents the numerical simulation results for all the values of J.

It is evident from Figure 12 that the most important features of the represented transmission specters are the following:

- Four transmission peaks are observed in the studied spectral range for $J \geq 2$.
- The minimal transmission $T_{min}\%(0.5\mu m)$ at $\lambda = 0.5$ μm and the average full width at half maximum (FWHM) $\Delta\lambda$ (μm) of the peaks decrease with J increasing.

As we can see from Figures 13 and 14 which respectively illustrate the behaviour of the $T_{min}\%(0.5\mu m)$ and the (FWHM) $\Delta\lambda$ (μm) versus the repetition number J, the optimal value J which can be chosen for the study configuration $(PMS)^J[GCLM]^P(PMS)^J$ is $J \geq 5$. The value $J = 5$ corresponds to the minimal periodical (LH) number which can be traced to have minimal transmission 0.12% and the FWHM (3.8×10^{-4} μm). Indeed, from $J = 5$ no considerable improvement in the performances of the systems is observed compared with the cases $J = 2$, $J = 3$ and $J = 4$.

4.2.2 Numerical results of the study configurations: $H(LH)^5[GCLM]^PH(LH)^5$

Now we move on the discussion of the results of numerical calculation of transmission spectra for the study configuration S_P: $H(LH)^5[GCLM]^PH(LH)^5$.

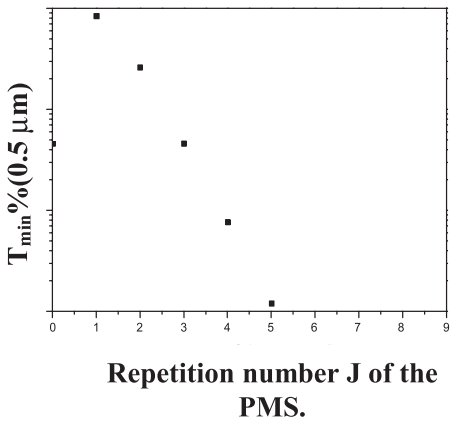

Fig. 13. Plot of the minimal transmission at λg 0.5 μm versus repetition number J for the $H(LH)^J(HLH3LHLH)^3H(LH)^J$ structure.

As we have seen in Section 4.2.1, the parameters a, b and m respect the inequality: $a + b < m$.

To compare the performances of the studied structures, we follow the evolution of these parameters in each structure:

- The number of the Bragg peaks.
- The minimal transmission between the peaks, which should be the weakest.
- The maximal transmission of the peaks, which must reach the 100%
- The average of full width at half maximum (FWHM) of the peaks, which should be the sharpest.
- The peak positions.

According to the obtained results, we notice that when m is even, the distributions of the peak positions versus the repetition number p commonly is given by the Figure 15.

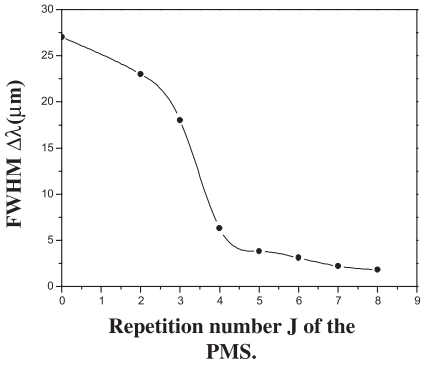

Fig. 14. Plot of the average of the full width at half maximum (FWHM) of the peaks versus the repetition number J of the $H(LH)^J(HLH3LHLH)^3H(LH)^J$structure.

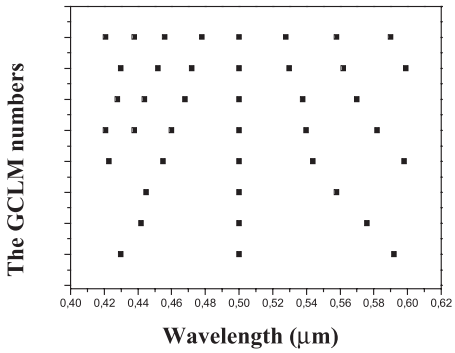

Fig. 15. Plot of the peak positions versus repetition number P of the $H(LH)^5[H2LH]^PH(LH)^5$ structure.

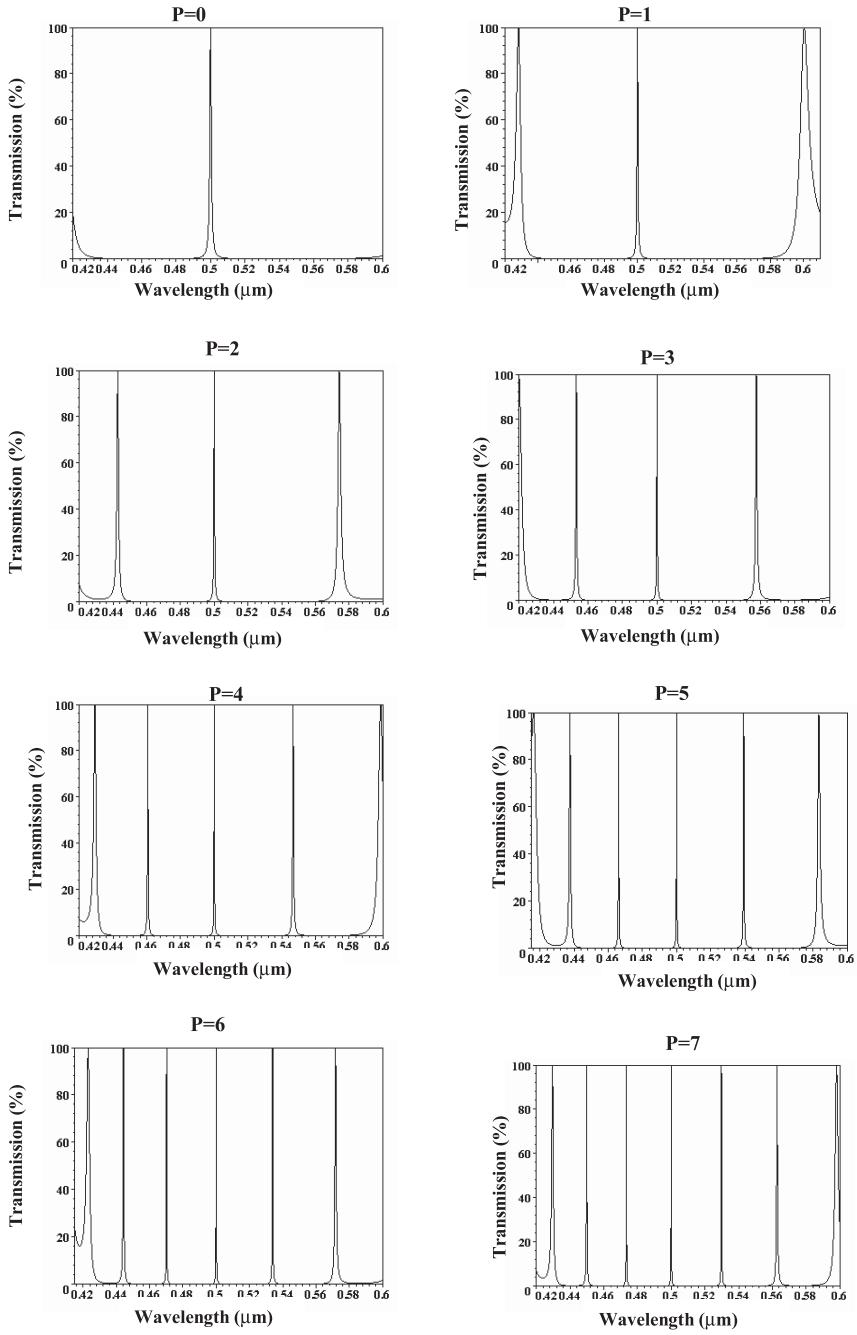

Fig. 16. Transmission spectrum versus wavelength for the $H(LH)^5[H2LH]^PH(LH)^5$ structure for different P values.

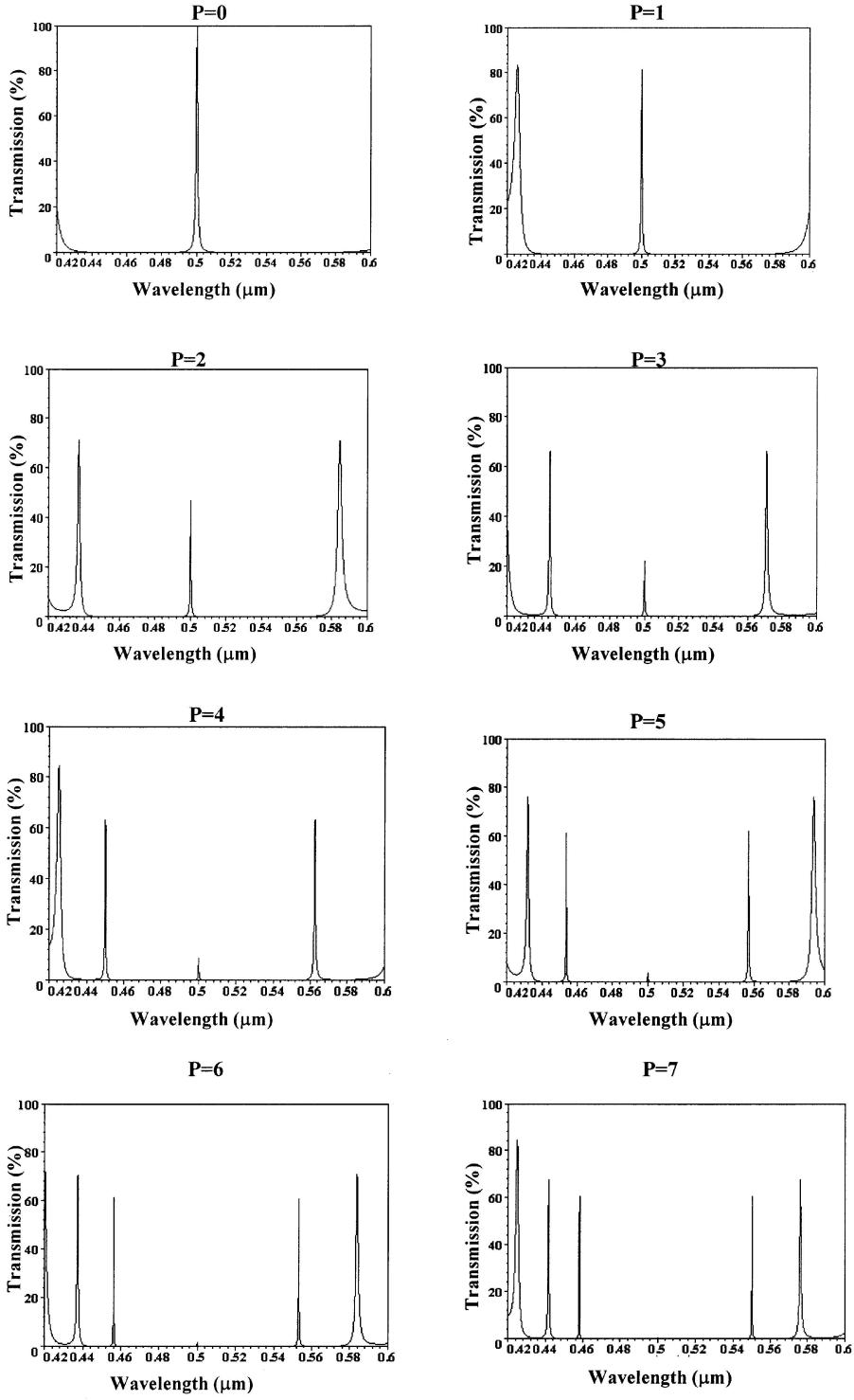

Fig. 17. Transmission spectrum versus wavelength for the $H(LH)^5[2HLH]^P H(LH)^5$ structure for different P values.

Note the presence of the peak at $\lambda = \lambda_0 = 0.5$ μm for every value of P. The best results which correspond to 100% transmission of peaks are obtained only for symmetrical structures (GCLM) of type $aH\ bL$ aH with $b = m - 2a$. For example Figure 16 illustrates the case which correspond to $m = 4$, $a = 1$ then $b = 2$ and the (GCLM) structure concerned is H2LH. In the case of the asymmetrical structures such as $aH\ bL[m-(a+b)]H$ one notes in general a decrease until zero of the transmission peaks at $\lambda = \lambda_0 = 0.5$ μm as it is shown by Figure 17 for $m = 4$, $a = 2$ and $b = 1$. Besides, the other peak intensities keep values between 60 and 80%.

For the case m an odd number, the distributions of the peak positions versus the repetition number P is given by Figure 18. Note the absence and the presence of the peak

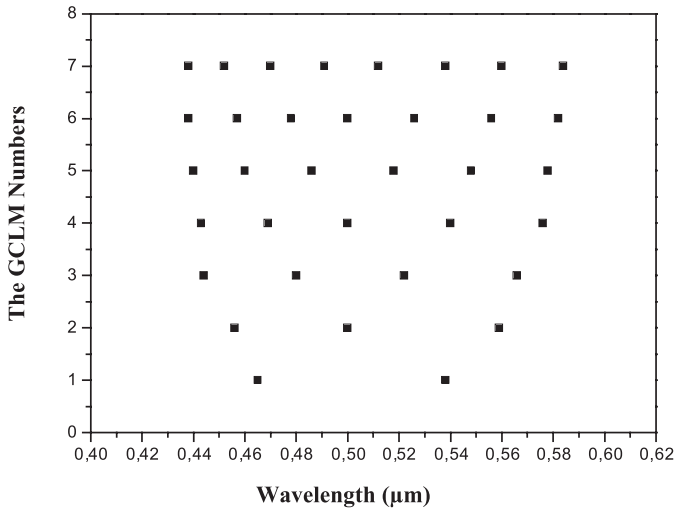

Fig. 18. Plot of the peak positions versus repetition number P of the $H(LH)^5[H3LH]^PH(LH)^5$structure.

at $\lambda = \lambda_0 = 0.5$ μm. Indeed, if we use ON to represent the maximal transmission and OFF the minimal one at $\lambda = \lambda_0 = 0.5$ μm, the coefficient transmission T through the structures, has the following switch like properties (see Fig. 19):

S_0(ON)-S_1(OFF)-S_2(ON)-S_3(OFF)-S_4(ON)-S_5(OFF)...

Note that we do not observe in this case a great difference between geometrical and spectral properties, although we show that the best performances are obtained for the symmetrical configurations. However, the odd values of m give interesting results, in particular the switching phenomena observed at $\lambda = \lambda_0 = 0.5$ μm:

In order to check the predicted scaling of the transmission spectra at $\lambda = \lambda_0$, we use the antitrace map method [16] to evaluate the transmission coefficients through a considered structure. The trace-map technique, first introduced in 1983 [17], has proven to be a powerful tool to investigate the properties of various aperiodic systems. However, we must know the so-called "antitrace map" when we evaluate the light transmission coefficients through an aperiodic sequence [18]. Here the so-called "antitrace" of a 2×2 matrix $A = \begin{pmatrix} A_{11} & A_{12} \\ A_{21} & A_{22} \end{pmatrix}$ is defined as $y_A = A_{21} - A_{12}$.

We use the antitrace map method to evaluate the transmission coefficients at $\lambda = \lambda_0$, through a $H(LH)^5[H3LH]^PH(LH)^5$, $H(LH)^5[2HLH]^PH(LH)^5$ and $H(LH)^5[H2LH]^PH(LH)^5$ structures which have the following properties:

– For the structure $H(LH)^5(H3LH)^P$ $H(LH)^5$:

S_0(ON) - S_1(OFF)- S_2(ON) - S_3(OFF)- S_4(ON) - S_5(OFF)...

– For the structure $H(BH)^5(2HLH)^PH(BH)^5$:

S_0(ON) - S_1(ON)- S_2(ON) - S_3(ON)- S_4(ON) - S_5(ON)...

while the peak intensity decreases with P increases.

– For the structure $S_p = H(LH)^5(H2LH)^PH(LH)^5$:

S_0(ON) - S_1(ON)- S_2(ON) - S_3(ON)- S_4(ON) - S_5(ON)...

We always have 100% transmission independently of the value of P.

Each of the homogeneous layers is characterised by the following matrix [14]:

$$M_i = \begin{pmatrix} \cos\varphi_i & \frac{j}{n_i}\sin\varphi_i \\ jn_i\sin\varphi_i & \cos\varphi_i \end{pmatrix}$$

where M_i is the characteristic matrix of the ith layer and $\varphi_i = \frac{2\pi}{\lambda} n_i d_i$, d_i is the thickness of the ith layer and n_i is the refractive index of the ith layer. The matrix M_i is unimodular.

The characteristic matrix of the overall multilayer system is given by:

$S_p = \prod_i M_i = \begin{pmatrix} S_{11} & S_{12} \\ S_{21} & S_{22} \end{pmatrix} MA^pM$, where M = matrix product of $H(LH)^5$ structure and A^P = matrix product of $A_1 = [H3LH]$, $A_2 = [2HLH]$ and $A_3 = [H2LH]$ structures.

Since S_p is unimodular transfer matrix, the transmission coefficient is given by [19]:

$$T = \frac{4}{|S_{ij}|^2 + 2} \tag{1}$$

which can be expressed in the following form:

$$T = \frac{4}{x_s^2 + y_s^2} \tag{2}$$

where x_s and y_s denote the trace and antitrace of the transfer matrix S_p, respectively.

From (2), we see that the transmission coefficient is completely determined by the trace and antitrace. In the following discussion we need to know the pth power of unimodular 2×2 matrix A, which can be written as [20]:

$$A^p = U_p(x_A)A - U_{p-1}(x_A)I \tag{3}$$

where I is the unit matrix and $U_p(x_A) = \frac{\lambda_+^p - \lambda_-^p}{\lambda_+ - \lambda_-}$, $\lambda_\pm = \frac{x_A \pm \sqrt{x_A^2 - 4}}{2}$.

Here x_A and $\lambda_\pm$ denote the trace and two eigen-values of A, respectively. Using equation (3), we can write the recursion relation of the transfer matrix S_p:

– For the A^p structure we have:

$$\begin{cases} x_{AS} = U_p(x_A)x_A - 2U_{p-1}(x_A) \\ y_{AS} = U_p(x_A)y_A. \end{cases}$$

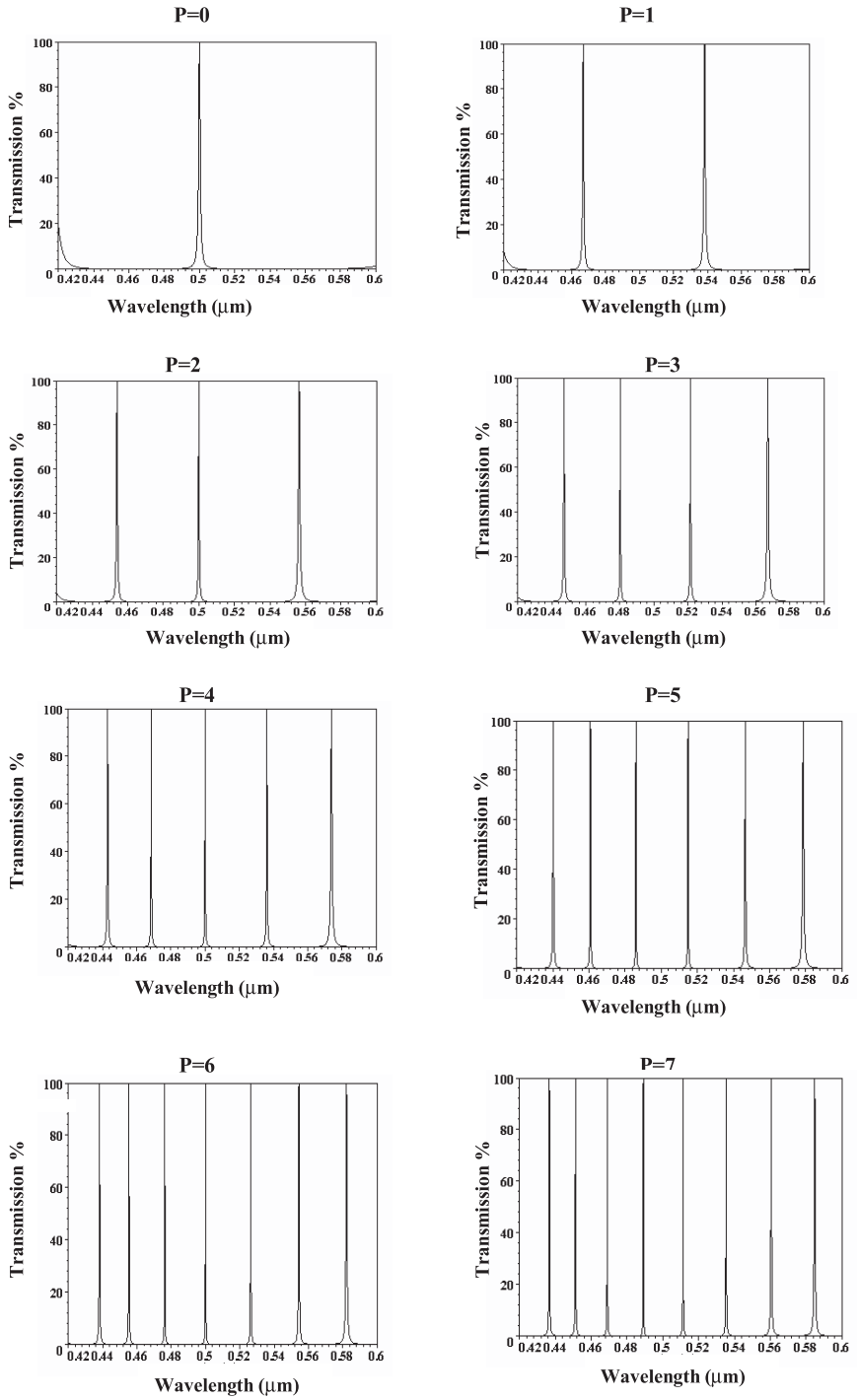

Fig. 19. Transmission spectrum versus wavelength for the $H(LH)^5[H3LH]^PH(LH)^5$ structure for different P values.

– For the MA^pM structure we have:
$\begin{cases} x_S = U_p(x_A)x_{MAM} - U_{p-1}(x_A)x_{M^2} \\ y_S = U_p(x_A)y_{MAM} - U_{p-1}(x_A)y_{M^2}. \end{cases}$

For $\lambda = \lambda_0$ we have: $M^2 = \begin{pmatrix} -1 & 0 \\ 0 & -1 \end{pmatrix}$, $MA_1M = \begin{pmatrix} 0 & \frac{j}{n_H}e'^9 \\ -jn_He^9 & 0 \end{pmatrix}$, $MA_2M = \begin{pmatrix} -e' & 0 \\ 0 & -e \end{pmatrix}$ and $MA_3M = \begin{pmatrix} -1 & 0 \\ 0 & -1 \end{pmatrix}$ where $e = n_H/n_L$ and $e' = n_L/n_H$. The results of the three structures $H(LH)^5[H3LH]^PH(LH)^5$, $H(LH)^5[2HLH]^PH(LH)^5$and $H(LH)^5[H2LH]^PH(LH)^5$are summarised in Tables 1, 2 and 3 respectively. For all the structures we classify the results into two classes, the even family with $p = 2m$ and the odd family with $p = 2m + 1$. For the even family, the transmission coefficients are 100%

Table 1. Trace, antitrace and transmission coefficients for the $H(LH)^5(H3LH)^PH(LH)^5$ structures.

p	0	1	2	3	4	5	6	7
$U_p(x_A)$	0	1	0	–1	0	1	0	–1
$U_{p-1}(x_A)$	1	0	1	0	–1	0	1	0
x_S	–2	0	2	0	–2	0	2	0
y_S	0	$-j146.199$	0	$+j146.199$	0	$-j146.199$	0	$+j146.199$
$T(\%)$	100	1.87×10^{-2}	100	1.87×10^{-2}	100	1.87×10^{-2}	100	1.87×10^{-2}

Table 2. Trace, antitrace and transmission coefficients for the $H\text{-}LH)^5(2HLH)^PH(LH)^5$ structures.

p	0	1	2	3	4	5	6	7
$U_p(x_A)$	0	1	2.2166	3.9135	6.4581	10.4020	16.5993	26.3927
$U_{p-1}(x_A)$	–1	0	1	2.2166	3.9135	6.4581	10.4020	16.5993
x_S	–2	–2.2166	–2.913	–4.2415	–6.4885	–10.1415	–15.9907	–25.3047
y_S	0	0	0	0	0	0	0	0
$T(\%)$	100	81.40	47.12	22.23	9.50	3.88	1.56	0.62

Table 3. Trace, antitrace and transmission coefficients for the $H(LH)^5(H2LH)^PH\text{-}LH)^5$ structures.

p	0	1	2	3	4	5	6	7
$U_p(x_A)$	0	1	2	3	4	5	6	7
$U_{p-1}(x_A)$	–1	0	1	2	3	4	5	6
x_S	–2	–2	–2	–2	–2	–2	–2	–2
y_S	0	0	0	0	0	0	0	0
$T(\%)$	100	100	100	100	100	100	100	100

for the MA_1^pM structure and the MA_3^pM one, and decrease from 100% to 0 for the MA_2^pM structure. For the odd family, the transmission coefficients are $1.87 \times 10^{-2}\%$ and 100%, respectively for MA_1^pM and MA_3^pM structures, and decrease from 81.40% to 0 for the MA_2^pM structure.. These results confirm very well the numerical calculations which are shown in Figures 6, 7 and 9.

5 Conclusion

Generalized Cantor systems can supply an interesting alternative to regular photonic crystals for the realization of photonic devices like dielectric mirror. Another interesting future application of these materials could be realized in the field of sensitive optical filters, where the resonance peaks observed in the reflection spectra could serve as the bases of the polychromatic filter device. One shows that more the one-dimensional generalized multilayer Cantor structures contain low refractive indices layers L, more the number of Bragg peaks increases. The latter are characterized by values adjoining the 100% reflection and are separated by transmission peaks with very weak values.

Multiple resonance peaks in the visible range are observed in the spectral visible range when a generalized Cantor multilayer is inserted between two highly reflective mirrors. The number of peaks is dependent on the repetition number P of the generalized Cantor like-multilayer. The transmission peaks can be made very sharp by increasing the reflectivity of the mirror and the repetition number P. The best performances are obtained only for the symmetrical configurations of the generalized Cantor multilayer and in particular for P an odd number. In any cases, the average of the full width at half maximum (FWHM) for each of the resonance peaks can be as narrow as possible with increasing P.

Finally, it is useful to note that all the results obtained are applicable not only to the generalized Cantor-like multilayer but probably for other quasi periodic systems such as (generalized Fibonacci sequences, generalized Thue-Morse sequences, ...) which constitute a perspective of this work.

References

1. O. Angelesky, A. Kovalchuk, P. Maksimyak, J. Opt. A: Pure Appl. Opt. **3**, 34 (2001)
2. J.N. Winn, Y. Fink, S. Fan, J.D. Joannopoulos, Opt. lett. **23**, 1573 (1998)
3. B. Temelkuran, E.L. Thomas, J.D. Joannopoulos, Y. Fink, Opt. Lett. **26**, 1370 (2001)
4. C. Sibilia, M. Scalora, M. Centini, M. Bertolotti, M.J. Bloemer, C.M. Bowden, J. Opt. A: Pure Appl. Opt. **1**, 490 (1999)
5. M. Bayindir, E. Ozbay, B. Temelkuran, M.M. Sigalas, C.M. Soukoulis, R. Biswas, K.M. Ho, Phys. Rev. B **63**, 081107 (2001)
6. M. Deopura, C.K. Ullal, B. Temelkuran, Y. Fink, Opt. Lett. **26**, 1197 (2001)
7. M.C. Parker, R.J. Mears, S.D. Walker, J. Opt. A: Pure Appl. Opt. 3, 171 (2001)
8. M. Centini, M. Scalora, C. Sibilia, G. D'Aguanno, M. Bertolotti, M.J. Boloemer, C.M. Bowden, J. Opt. A: Pure Appl. Opt. **2**, 121 (2000)
9. J. Lekner J. Opt. A: Pure Appl. Opt. **2**, 349 (2000)
10. M. Kohmoto, B. Sutherland, K. Iguchi, Phys. Rev. Lett. **58**, 2436 (1987)
11. R. Riklund, M. Sverin, J. Phys. C: Solid State Phys. **21**, 3217 (1988)
12. M. Bertolotti, P. Masciulli, C. Sibilia, Opt. Lett. **19**, 777 (1994)
13. M. Kanzari, B. Rezig, J. Opt. A: Pure Appl. Opt. **3**, S201 (2001)
14. F. Abelès, Ann. Phys. Paris **12**, 596 (1950)
15. T. Megademini, J. Phys. III France **3**, 321 (1993)
16. X.G. Wang, S.H. Pan, G.Z. Yang, Chin. Phys. lett. **18**, 80 (2001)
17. M. Komoto, L.P. Kadanoff, C. Tang, Phys. Rev. Lett. **50**, 1870 (1983)
18. M. Dulea, M. Severin, R. Riklund, Phys. Rev. B **42**, 3680 (1990)
19. M. Komoto, B.S. Sutherland, I. Iguchi, Phys. Rev. Lett. **58**, 2436 (1987)
20. M. Kolar, M.K. Ali, Phys. Rev. B **41**, 7108 (1990)